THE PENNSYLVANIA STATE UNIVERSITY
SCHREYER HONORS COLLEGE

Engineering 2-D Materials from Molybdenum Aluminum Boride

OWEN ADAMS
SPRING 2025

A thesis
submitted in partial fulfillment
of the requirements
for a baccalaureate degree
in Mechanical Engineering
with honors in Mechanical Engineering

Reviewed and approved* by the following:

Raymond Schaak
Dupont Professor of Materials Chemistry
Thesis Supervisor

Jean-Michel Mongeau
Shuman Family Assistant Professor of Mechanical Engineering
Thesis Honors Adviser

* Electronic approvals are on file.

ABSTRACT

As the demand for reliable energy storage increases, there is a need to improve current battery technology. One method to do so is by replacing graphene, a 2-D material commonly used in lithium-ion batteries (LIBs), with other emerging 2-D materials. This interest in 2-D materials calls for synthesis of new compounds which can be reduced to their 2-D counterparts. One such material, MoAlB, is herein synthesized and investigated. Two new synthetic pathways to Mo_2AlB_2, a metastable phase between MoAlB and 2-D MoB, were developed and refined. These pathways provide a more favorable route for continued aluminum removal toward 2-D MoB, which has favorable electrical and mechanical properties for applications in batteries and other energy storage devices.

TABLE OF CONTENTS

LIST OF FIGURES……..iii

LIST OF TABLES.....iv

ACKNOWLEDGEMENTS.....v

Chapter 1: Introduction 1

1.1 Introduction 1
1.2 Batteries: Fundamentals and lithium-ion battery shortcomings.....1
1.3 Graphene and other 2-D materials 3
1.4 MAX phases and 2-D MXenes.....4
1.5 MAB phases and 2-D MBenes.....8
1.6 The work of this thesis 10

Chapter 2: Experimental Methods and Materials 11

2.1 Introduction 11
2.2 Chemicals and Materials.....11
2.3 MoAlB bulk powder synthesis.....12
2.4 Mo_2AlB_2 Synthesis via Lewis acid salt reaction.....12
2.5 Mo_2AlB_2 synthesis using iodine.....13
2.6 Etching.....14
2.7 Characterization 14

Chapter 3: Results and Discussion.....16

3.1 Introduction 16
3.2 Mo_2AlB_2 from topochemical transformation of MoAlB using $ZnCl_2$ and other metal chloride salts.....16
3.3 Mo_2AlB_2 from reaction with I_2 21
3.4 Etching aluminum from Mo_2AlB_2.....25

Chapter 4: Conclusion.....29

Appendix A: Justification for Metal Chloride Salt Selection.....31

Appendix B: Simulating Preferred Orientation on Reference Patterns for MoAlB and Mo_2AlB_2 33

BIBLIOGRAPHY 35

LIST OF FIGURES

Figure 1. Simple battery structure with electron flow from cathode to anode causing an electrical potential while ions are transported through the electrolyte.....2

Figure 2. General MAX phase selective etching process to reach MXenes. Adapted with permission from Chaudhari et al.[13] 5

Figure 3. Crystal structures of MoAlB (left) and Mo_2AlB_2 (right). Adapted from Baumler et al.[40] 9

Figure 4. Powder XRD patterns of Mo_2AlB_2 (purple) synthesized by reacting MoAlB (blue) with $ZnCl_2$ at 550°C for 170 hours. Reference patterns based on published crystallographic data for MoAlB[43] and Mo_2AlB_2[39] and adjusted to account for preferred orientation (Appendix B) are shown. Adapted from Baumler et al.[40] 17

Figure 5. Powder XRD patterns of products of MoAlB and the four selected metal chloride salts. Reference patterns for MoAlB[43] and Mo_2AlB_2[39] are shown and experimental peaks are matched to one of these two patterns. Adapted from Baumler et al.[40].....19

Figure 6. Powder XRD patterns of Mo_2AlB_2 from reaction of MoAlB with $ZnCl_2$ and I_2. Reference patterns for MoAlB[43] and Mo_2AlB_2[39] are shown.....22

Figure 7. Powder XRD temperature series patterns of the products of I_2 reactions with MoAlB from 300 °C – 800 °C for 16 hours. Reference patterns for MoAlB[43] and Mo_2AlB_2[39] are included.....24

Figure 8. Powder XRD patterns of the products of Mo_2AlB_2 stirring in HCl and NaOH. The pattern of the starting Mo_2AlB_2 sample and the reference pattern for Mo_2AlB_2[39] are included. 26

Figure 9. (a) SEM image of etched Mo_2AlB_2 from stirring Mo_2AlB_2 in 2M HCl. (b) SEM image of etched Mo_2AlB_2 from stirring Mo_2AlB_2 in 10 weight-percent NaOH. 27

Figure B1. Powder XRD patterns of Mo_2AlB_2 (purple) synthesized by reacting MoAlB (blue) with $ZnCl_2$ at 550°C for 170 hours. Reference patterns based on published crystallographic data for MoAlB[41] and Mo_2AlB_2[37]. Modeled patterns display preferred orientation in 0k0 for MoAlB and 021 for Mo_2AlB_2. Adapted from Baumler et. Al.[38] 33

LIST OF TABLES

Table A1. Summary of selected metal chloride salts based on melting point[43] and reactivity, which is determined by redox potential, E(V). 31

Table A2. Calculations for Redox Potentials of Selected Metals and Chlorine with Aluminum. 32

ACKNOWLEDGEMENTS

Thank you to Dr. Schaak for providing a first year Mechanical Engineering student the opportunity to explore the wonders of solid-state chemistry. Dr. Schaak has consistently been an approachable and compassionate research advisor, empowering me to become the researcher, writer, and creative mind that I am today. I would also like to thank Dr. Schaak, and all other members of the Schaak lab, for providing a safe and welcoming environment to do chemistry.

I would like to give special thanks to Dr. Kate Baumler, who always took the time to help me with my research and answer my questions. Dr. Baumler has been an invaluable mentor over the last three years, helping me navigate my undergraduate career and the entrance process to graduate studies. Most of all, Kate has been a friend, and I will cherish all the laughs we've shared over the years.

Chapter 1:

Introduction

1.1 Introduction

One of the most pressing issues of our society is that of climate change. While renewable energy sources, such as wind and solar, offer a promising path to reducing global energy consumption, these energy sources are not continuous. As a result, effective widescale grid energy storage is integral to transitioning to renewable energy and slowing the devastating impacts of climate change. Current grid-scale energy storage is dominated by pumped hydroelectric, but batteries are recognized as a viable supporting option.[1] Batteries are also used extensively for smaller scale applications of everyday life.[2] Therefore, batteries play a critical role in our lives and the lives of future generations.

1.2 Batteries: Fundamentals and lithium-ion battery shortcomings

A battery is a type of galvanic cell undergoing a spontaneous redox reaction to produce an electrical potential.[3] A battery consists of two electrodes: the anode is where oxidation occurs, and the cathode is where reduction occurs. An electrolyte substance, which is composed of an ionically conductive material, surrounds the anode and cathode and is used for ion transport between the two electrodes (Figure 1).[2] As the redox reaction occurs, charge, in the form of electrons, is transferred, which results in an electrical potential, or voltage. Battery performance can be quantified in a few ways. One key indicator of battery performance is the capacity (mAh),

which denotes the amount of electrical charge that can be gained during charging, stored during the open-circuit state with no charging or discharging, and then released during discharge.[4] Another important measure of battery performance is the electrical potential (ΔV) across electrodes during charging and discharging or open circuit.[4]

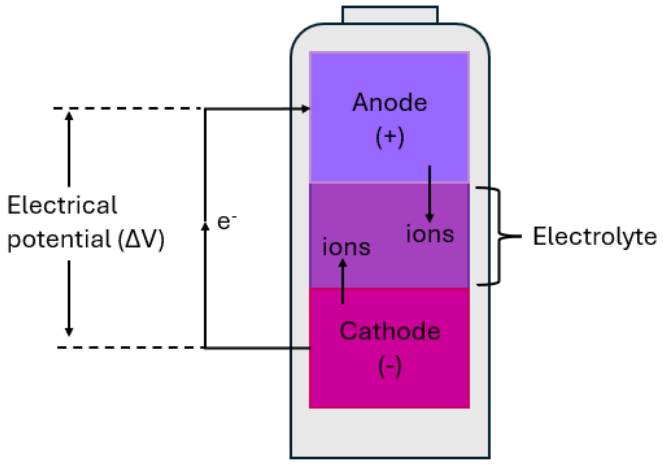

Figure 1. A simple battery structure with electron flow from cathode to anode causing an electrical potential while ions are transported through the electrolyte.

Capacity in batteries can be increased by improving the surface-area to-mass ratios in electrodes, and the electrical potential can be increased by adjusting the chemical composition of electrodes.[2] Compared to previous options, such as lead-acid or Ni-Cd batteries, lithium-ion batteries (LIBs) not only display higher capacities and electrical potentials, but also facilitate reversible Li^+ ion interaction at both electrodes, which improves battery life.[2] However, LIBs pose safety concerns due to their combustibility and impose a large carbon footprint during their production. Because of these shortcomings, there is a need to engineer new technology to improve LIBs to function at higher efficiency until an alternative is found.[2]

1.3 Graphene and other 2-D materials

2-D materials are those which are only a few atoms thick.[5] These ultra-thin materials have high surface-area-to-mass ratios, which indicates a high capacity value and makes them favorable materials for many energy storage applications.[2,6] Graphite, a 3-D crystalline material which was used in the first LIBs, has now been engineered down to a single 2-D layer, graphene.[7] In addition to the characteristic high surface-area-to-mass ratio of 2-D materials, graphene has high electrical conductivity, mechanical strength, and flexibility. As a result, graphene has applications in multiple important areas of energy storage, such as batteries, supercapacitors, solar fuel cells, and hydrogen generation devices.[6] Specific to batteries, LIB anodes with 2-D graphene have been experimentally determined to have a high reversible specific capacity of 1500 $mAhg^{-1}$.[7] Graphene's desirable properties have led it to being used extensively in LIB electrodes in the past decades. However, the favorable properties of graphene in LIBs are highly dependent on achieving high-quality, 2-D nanosheets of graphene.[6] This calls to the importance of the chemical synthesis of graphene toward creating more efficient energy storage devices.

Cost and scalability are two large obstacles for graphene synthesis which must be balanced with the quality of the synthesized material.[6] While complicated and expensive synthesis methods, such as chemical vapor deposition[5] and photoexfoliation[8], often yield high-quality graphene, these methods lack the scalability that is needed to produce graphene in bulk. Liquid-phase exfoliation is an alternative route toward graphene which uses sonication in aqueous conditions to peel away the layers of graphite to reach 2-D graphene.[9] This exfoliation method is promising due to its low cost and easy scalability, but it often results in impure

graphene with less favorable material properties.[5] Therefore, in addition to developing the exfoliation methods on 3-D graphite, it is worth considering what other 2-D materials are predicted to have favorable electrical and mechanical properties and how these materials can be synthesized from their 3-D starting materials.

1.4 MAX phases and 2-D MXenes

Similarly to graphite being chemically manipulated down to a single 2-D layer of graphene, a relatively new family of materials, MAX phases, can be engineered to single 2-D layers called MXenes.[10] MAX phases and MXenes have gained significant traction in the field of 2-D materials, largely because of the exciting properties of MXenes for electronic and energy applications.[11] MAX phases, the precursors to MXenes, consist of a M-element (an early transition metal), an A-element (an interleaving metal, often aluminum), and a X-element (carbon or nitrogen).[10] Upon selectively etching away the A-element, and exfoliating, or separating, the remaining MX layers, a 2-D MXene is reached. Selective etching, illustrated in Figure 2, means engineering a reaction pathway to extract the A-element from the 3-D MAX phase structure using topochemistry. This chemistry is possible because the bond strength between the M-and-X-element is much higher than the A-element, meaning that these bonds will remain intact while the A-element is etched.[12]

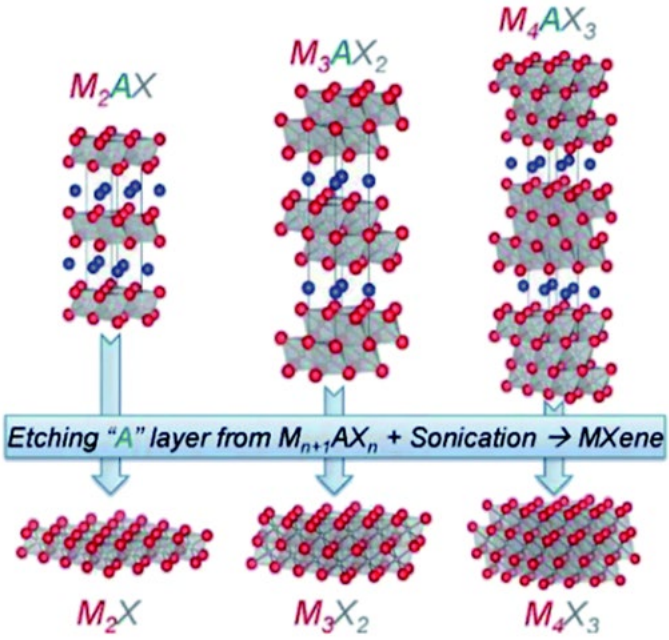

Figure 2. General MAX phase selective etching process to reach MXenes. Adapted with permission from Chaudhari et al.[13]

While MXenes share the high surface-area-to-mass ratio common among 2-D materials which indicates high electrical capacities, they also possess unique properties that separate them from graphene and other 2-D materials. Based on the definition of MAX phases, there is variability in each of the three elements that make up a MAX phase. As a result, there are a plethora of possible MAX phases, each of which have a potential MXene counterpart with different properties. In addition, MAX phases with the same elements can have different stoichiometries (Figure 2), which can lead to additional differences in properties. As a result of the tunability of elemental composition and stoichiometry in MXenes, across the family of MXenes there is a large range of operating electric potentials.[10] This range of potentials is exciting for battery applications, allowing some MXenes to function as cathodes[14,15] while others function as anodes.[16,17,18] In addition to high capacity and wide structural variety, MXenes have

been shown to have cyclability and stability in batteries, making them a promising group of 2-D materials for energy storage applications.[10] In addition to electric properties for energy storage applications, the wide compositional variety of possible MXenes allows for tunability of their mechanical properties. MXenes have been reported to have the highest stiffness among 2-D materials that are solution-processed.[19] Furthermore, varying thicknesses of 2-D MXenes due to stoichiometric differences of synthesizable MAX phases can lead to a high level of tunability in the stiffness and flexural strength of MXenes.[19,20] With many different MAX phases and accompanying differences in properties and reactivity, a wide range of synthesis and etching reactions have been explored in hopes of continuing to create more 2-D MXenes with highly favorable properties.

These desirable properties of MXenes can only be tested and confirmed once a MAX phase has been engineered down to 2-D layers. Therefore, the starting point for any MXene is the synthesis of the MAX phase. MAX phases can be made in a few different ways. MAX phase synthesis using a hot press[21] or spark-plasma sintering[20] has shown to be effective, but the apparatuses needed impose a high entry cost.[22] More scalable and lower-cost methods have been developed for MAX phase synthesis, with self-propagating high-temperature synthesis[23] and molten-salt synthesis[24] methods leading the charge. A common theme among all synthetic methods is using a high temperature (> 1000 °C) and achieving a pure 3-D MAX phase that can be effectively manipulated in subsequent steps.

Once synthesized, MAX phases are commonly etched using strong fluoride-based aqueous solutions such as hydrofluoric acid (HF), but these reactions can damage the MXene product and hinder its electrochemical properties.[25] Milder reagents like hydrochloric acid (HCl) have successfully been used to etch MAX phases, with the product showing improved energy

storage and capacitance properties compared to HF-etched MXenes.[25] A Lewis acid approach has been shown to successfully etch the A-element through a less invasive reaction pathway.[26] In 2020, this Lewis acid etching approach was performed on Ti_3AlC_2 using $ZnCl_2$ as the Lewis acid salt, which resulted in the highest reported discharge capacity of the Ti_3C_2 MXene in a non-aqueous Li-ion electrolyte to date with a specific capacity value of 205 $mAhg^{-1}$.[27] These findings highlight the significance of the selective etching method used on MAX phases and the subsequent surface structure of the 2-D MXenes.

This surface structure plays a large role when further modifying the MXene structure by intercalating MXenes to exfoliate, or separate, the 2-D layers and reach a single layer. In common MAX phase reaction pathways, terminating groups from the etching reagent as well as oxygen are on the surface of each layer of the 2-D MXene.[28] These terminating groups increase the bonding strength between the layers and makes them hard to separate, but intercalants such as dimethyl sulfoxide (DMSO)[29] and tetrabutylammonium hydroxide (TBAOH)[30] allow for successful intercalation and delamination to reach a single-layer material. When put under galvanostatic charge-discharge cycling and at a cycling rate of 60 minutes, the specific capacity of the DMSO-delaminated single-layer Ti_3C_2 MXene in Li^+ ions was 410 $mAhg^{-1}$.[29] The high electric capacity of single-layer Ti_3C_2 makes it even more favorable as anodes in LIBs than was computationally predicted.[29] Surface structure also has a large impact on the mechanical properties of MXenes, and surface terminations have been reported as a method to tune mechanical stiffness.[19] Because of the exciting electric and mechanical properties of single-layer, delaminated MXenes, there is ongoing work on delaminating different MXenes as well as other 2-D layered materials.

1.5 MAB phases and 2-D MBenes

As the research on MAX phases and MXenes continues, a sister family of materials has emerged: MAB phases. The elemental breakdown of MAB phases matches MAX phases except for the B-element, boron, which replaces the carbon or nitrogen in MAX phases. The A-element in MAB phases can be selectively removed to reach 2-D MBenes, which are analogous to MXenes for MAX phases.[31,32] Multiple MBenes (Cr_2B_2, Fe_2B_2, Mn_2B_2, Mo_2B_2, and V_2B_2) have been theoretically predicted to demonstrate high electrical conductivity and storage capacity, and excellent stability.[33–35] Similarly to MXenes and graphene, MBenes also possess favorable mechanical properties. MBenes are reported to have ultra-high Youngs modulus which correlates to high stiffness.[33] MBenes also display tunability of mechanical properties and are predicted to be used in 2-D magnets.[36] These predictions demonstrate the appeal of MBenes in a wide range of engineering applications. However, the focus has only shifted to MAB phases more recently because of the success in MAX phase and MXene synthesis, calling for the continued expansion of synthesized 2-D materials. Many predicted MAB phases and MBenes, however, have yet to be synthesized.[35] MAB phases cannot withstand the harsh etching methods typically used on MAX phases, and will completely break down when reacted with HF.[37] Therefore, there is demand to engineer innovative reaction pathways to successfully synthesize and etch MAB phases to explore their mostly untapped potential in energy storage applications.

The Schaak Group has been intrigued by the unique properties and synthetic challenges associated with MAB phases and has made multiple findings related to the MAB phase MoAlB. In 2018, Alameda *et. al.* reported a method for topochemical deintercalation of aluminum from

MoAlB and observed an isolated 2-D MoB monolayer, which supported the feasibility of synthesizing a MoB MBene.[38] Additionally, topochemical reactions between MoAlB and $ZnCl_2$ or NaOH have been used to successfully synthesize Mo_2AlB_2, a metastable phase that is predicted to be a more suitable MBene precursor than MoAlB.[39,40]

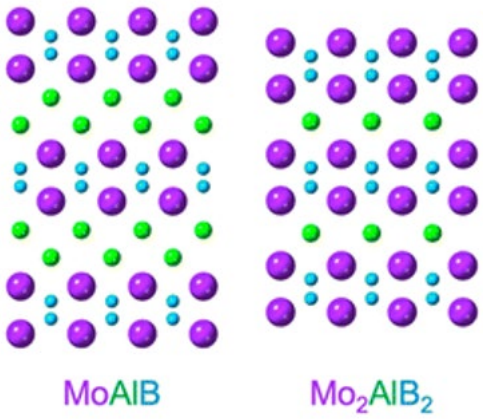

Figure 3. Crystal structures of MoAlB (left) and Mo_2AlB_2 (right). Adapted from Baumler et al.[40]

The difference between MoAlB and Mo_2AlB_2, highlighted in Figure 3, is that Mo_2AlB_2 has only one layer of aluminum between each MoB layer, whereas MoAlB has two layers of aluminum. With only one layer of aluminum, Mo_2AlB_2 has intrinsic structure and properties that separate it from MoAlB. Mo_2AlB_2 possesses a slight shift in the MoB layers compared to MoAlB because this intermediate phase stabilizes in a different structure. Additionally, Mo_2AlB_2 displays weakened bond strength between the aluminum layers and MoB layers compared to MoAlB.[33,38] Despite success in synthesizing materials like Mo_2AlB_2, which are predicted to be precursors to 2-D MBenes, successful engineering of a 2-D MBene has been elusive thus far. To date, there have only been two reported cases of successful removal of all aluminum in the system. Zhou *et. al.* was one of the first to report a successful 2-D molybdenum-based MBene, or "boridene", but their etching method involves HF which appears to only work on a few select MAB phases

($(Mo_{2/3}Y_{1/3})_2AlB_2$ and $(Mo_{2/3}Sc_{1/3})_2AlB_2$).[32] Wang *et. al.* also report the complete removal of aluminum from Ti_2InB_2 using a dealloying strategy, but the high temperature of this etching process prevented the yield of a 2-D material.[31] Others have reported molybdenum-based 2-D MBenes, but critical analysis of the reported data indicates they are often yielding $MoAl_{1-x}B$ or a product that has experienced corrosive reactions instead of topochemical etching. Therefore, a deeper understanding of the reaction mechanisms of MoAlB appears necessary to successfully engineer its 2-D MBene counterpart.

1.6 The work of this thesis

Motivated by the promising applications of 2-D MBenes as electrode materials in batteries, this thesis documents the work toward the synthesis of 2-D MoB, which is derived from the MAB phase MoAlB. The research of this thesis involves the exploration of different reaction pathways to anticipated 2-D MoB precursors, namely Mo_2AlB_2, as well as different etching methods towards the MoB MBene. This work provides novel insight into the sensitive reaction mechanisms of MAB phases and their 2-D counterparts, the latter of which hold significant potential for improving batteries and other energy-related devices because of their desirable electrical and mechanical properties.

Chapter 2:

Experimental Methods and Materials

2.1 Introduction

This chapter focuses on the experimental methods for multiple key reactions involving the MAB phase MoAlB to better understand the reaction pathway toward the 2-D MBene. Additionally, the chemicals and materials used for these reactions are listed in the first section. Next described is the synthesis of MoAlB, the primary starting material for all subsequent reactions towards the 2-D MoB. This synthetic approach was taken from Alameda *et al.*[39] After MoAlB synthesis, two different methods for the synthesis of Mo_2AlB_2 are presented, both of which have not been previously reported on MoAlB and were developed in collaboration with Kate Baumler and Raymond Schaak. Lastly, this chapter reports an etching reaction to remove additional aluminum out of Mo_2AlB_2. This etching reaction is once again previously unreported and developed in collaboration with Kate Baumler and Raymond Schaak.

2.2 Chemicals and Materials

Molybdenum boride powder (MoB, -325 mesh, 99% purity) was purchased from Alfa Aesar. Aluminum chips (Al, 99.99% purity) about 1 mm thick and 12 mm in diameter were purchased from NOAH Technologies and were cut into smaller chunks using bolt cutters to be loaded into the ceramic boats. Zinc chloride powder (ZnCl2, ≥ 97% purity), lithium chloride powder (LiCl, ≥ 99.0% purity), nickel chloride powder (NiCl2, 98% purity), and iodine flakes

(I_2, ≥ 99.0% purity) were purchased from Sigma Aldrich. Sodium chloride powder (NaCl, GR ACS) was purchased from EMD Millipore Corporation. Alumina crucibles and boats were purchased from CoorsTek.

2.3 MoAlB bulk powder synthesis

The first step toward the synthesis of 2D MoB or its predicted metastable precursor, Mo_2AlB_2, is the bulk synthesis of MoAlB powder.[33] To synthesize MoAlB, Al chips were added to MoB powder in a 2 mL crucible in 2 gram batches with a molar ratio of 1:1.3 MoB to Al.[39] Multiple of these crucibles were placed in a mullite tube furnace (Carbolite STF 15/180) under argon flow and heated at 1400 °C for 10 hours before reducing the temperature to 900 °C at a rate of 60 °C/hour, then quickly cooling to room temperature. The MoAlB product was then crushed with a hammer and ground to a powder using an agate mortar and pestle.[39]

2.4 Mo_2AlB_2 Synthesis via Lewis acid salt reaction

Mo_2AlB_2 was synthesized through a Lewis acid salt reaction involving MoAlB and $ZnCl_2$.[40] To reach Mo_2AlB_2, MoAlB powder was heated with ten times excess $ZnCl_2$ based on previous work involving Lewis acid salt reactions with MAX phases.[26] Due to the low melting point of $ZnCl_2$ (290 °C), it was not necessary to press or grind the reactants together before heating.[41] The MoAlB powder was placed in a porcelain boat with ten times excess $ZnCl_2$ added on top, and the boat was put into a quartz single-zone tube furnace (Lindberg/Blue Mini-Mite) under nitrogen gas flow. After a 30-minute purge period under nitrogen flow, the reactants were

then heated to 550 °C for 170 hours with at least a 1-hour ramp up period.[40] The furnace was then turned off and allowed to cool to room temperature. Following the reaction, the sample was washed with water and centrifuged three times at 14500 RPM for 2 minutes to remove any excess zinc chloride. The sample was then dried to a powder under forced air.

To help further understand the driving forces of the zinc chloride reaction towards Mo_2AlB_2, reactions of three other metal chloride salts, NaCl, LiCl, and $NiCl_2$, were conducted. The reaction of these metal chloride salts, of general composition MCl_x, with MoAlB mirrored that of the $ZnCl_2$ reaction. After adding ten times excess MCl_x to MoAlB powder in a porcelain boat, this mixture was added to a quartz single-zone tube furnace (Lindberg/Blue Mini-Mite) under nitrogen gas flow. The reaction was heated to 650 °C for 1 hour (or 36 hours in the case of NaCl) following a 30-minute purge period. The furnace was then allowed to cool before the sample was removed and washed with water. Further justification for the selection of metal chloride salts can be found in Appendix A.

2.5 Mo_2AlB_2 synthesis using iodine

Another pathway to Mo_2AlB_2 is through a reaction with iodine. In this reaction, MoAlB and 1.2 times the amount of I_2 needed to react all the aluminum to make AlI_3 was added to a quartz ampule, and then flame sealed under vacuum. The latter step is necessary because elemental iodine quickly volatizes in air which could inhibit the reaction under standard conditions. The rest of the reaction follows the same steps of the $ZnCl_2$-based reaction. The ampule was placed into a quartz single-zone tube furnace (Lindberg/Blue Mini-Mite) and put under nitrogen flow for 30 minutes before heating to around 300 °C-800 °C (in 100 °C

increments) for 16 hours. After the product was allowed to return to room temperature through a rapid cool-down, the product was washed with ethanol and centrifuged three times at 14500 RPM for 2 minutes to remove any excess I_2.

2.6 Etching

To attempt to further etch aluminum out of Mo_2AlB_2, the Mo_2AlB_2 produced from reacting MoAlB and iodine, detailed in the above section, was stirred in acid (HCl) and base (NaOH). To accomplish this, the Mo_2AlB_2 product was split in half and placed in two vials. In one vial, 10 mL of 10 weight-percent NaOH was added. 10 mL of 2 M HCl was added to the other vial. The samples were then stirred overnight for 22 hours. Following this stir, the etched samples were washed with water and centrifuged three times at 14500 RPM for 2 minutes before being dried under forced air.

2.7 Characterization

To analyze the products of the reactions described above, multiple characterization tools were used in the Materials Characterization Lab in the Millenium Science Complex at Penn State University. Powder X-ray diffraction (XRD) was conducted on a Malvern Panalytical Empyrean diffractometer using a copper K-alpha radiation source. Reference patterns for comparison to XRD results were simulated using CrystalDiffract® software[42] along with experimentally determined crystallographic data for MoAlB[43] and Mo_2AlB_2.[39] Additionally, CrystalMaker® software[44] was utilized to analyze the crystal structure of these MAB phase compounds.

Although XRD was the primary characterization method used for the work of this thesis, scanning electron microscopy (SEM) was also an important characterization method. SEM was performed on an ESEM Q250, which had a tungsten source and was operated at 20 kV. For higher resolution images, SEM images were obtained from a Verios G4 with a field emission gun source. To prepare for SEM characterization, samples were pressed into pellets and mounted on carbon tape or sprinkled directly onto the tape.

Chapter 3:

Results and Discussion

3.1 Introduction

In this chapter, the results of the experiments described in Chapter 2 are presented and critically analyzed. Much consideration is given to the synthesis of Mo_2AlB_2 through different reaction pathways, because this metastable phase is predicted to have a more favorable etching pathway towards the 2-D MBene.[39,40] Additionally, the results of etching reactions on Mo_2AlB_2 in hopes of removing further aluminum are discussed. These results provide further insight into the mechanisms that drive the etching of MAB phases toward their elusive 2-D counterparts, which possess promising characteristics for energy storage.[33–35]

3.2 Mo_2AlB_2 from topochemical transformation of MoAlB using $ZnCl_2$ and other metal chloride salts

As mentioned in Chapter 1.5, knowing that MAB phases cannot withstand the harsh etching reactions employed on MAX phases using HF, other reaction pathways must be explored. A published method to transform the MAX phases Ti_3AlC_2 and Ti_2AlC into their MXene counterparts in a less destructive manner uses a Lewis acid salt reaction between the MAX phases and $ZnCl_2$ with a stoichiometric ratio near 1:1 at 550 °C for 5 hours.[26] Molten $ZnCl_2$ has a strong Lewis acidity, meaning that the Zn^{2+} ion readily accepts electrons from the aluminum and replaces the aluminum between the titanium-carbon layers. This redox reaction, where Zn^{2+} reduces to Zn by accepting two electrons while Al loses electrons and oxidizes to

Al^{3+}, is favorable because of its positive redox potential. Under excess zinc chloride, this redox potential was reported to drive the reaction further by exfoliating the zinc to reach titanium-carbide MXenes.[26] Additionally, this topochemical process of etching MAX phases using a Lewis acid salt reaction was generalized to other metal salts so long as the redox pairs were favorable.[27] Testing this Lewis acid salt approach on a MAB phase, MoAlB, key differences were found in the reaction mechanism and product formed.

When reacted with MoAlB, instead of forming MoZnB or Mo_2ZnB_2, as would be the case for the analogous MAX phase reaction, $ZnCl_2$ instead worked to etch away half of the aluminum to reach metastable Mo_2AlB_2.[40] Powder XRD patterns of this Mo_2AlB_2 product and its MoAlB precursor are shown in Figure 4.

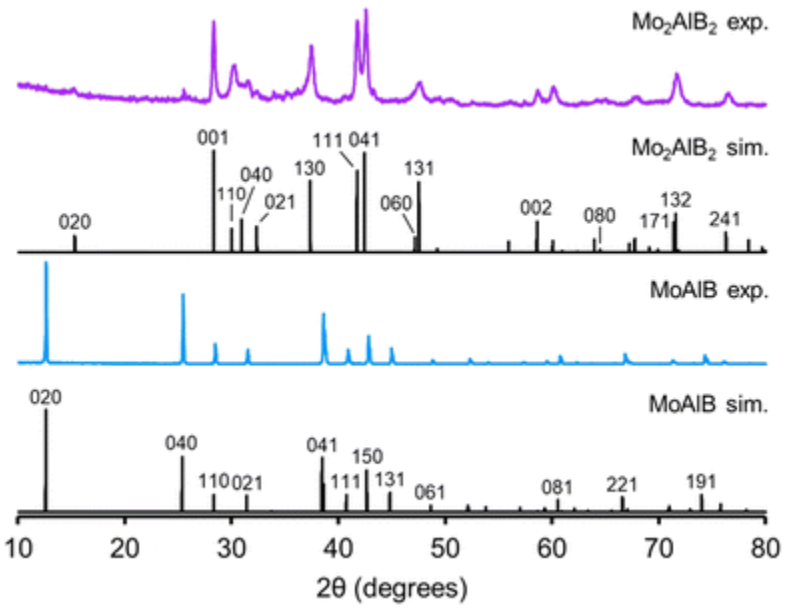

Figure 4. Powder XRD patterns of Mo_2AlB_2 (purple) synthesized by reacting MoAlB (blue) with $ZnCl_2$ at 550°C for 170 hours. Reference patterns based on published crystallographic data for MoAlB[43] and Mo_2AlB_2[39] and adjusted to account for preferred orientation (Appendix B) are shown. Adapted from Baumler et al.[40]

In Figure 4, the synthesized MoAlB matches the reference pattern[43] and displays preferred orientation in the *k*-direction because of the high peak intensity in the 020 and 040

peaks which are in the stacking direction of the crystal. The three numbers shown on top of each peak represent their miller indices in *hkl* crystallographic directions, which is analogous to *xyz*-coordinates in a standard 3-dimensional plane. This preferred orientation is expected, and it shows that the layers are stacked in an orderly manner on top of each other. Figure 4 also shows the product of MoAlB and $ZnCl_2$, which closely matches the reference pattern of Mo_2AlB_2[39] and demonstrates shifting of the 020 peak to 15.3° 2θ, precisely where it is expected to be for Mo_2AlB_2.[40] Stacking faults are also induced in the experimental Mo_2AlB_2 pattern because of the reaction's topochemical nature. The swapping of peak intensity of the two peaks around 43° 2θ is characteristic of such stacking faults (Appendix B). Small zinc oxide impurities are observed in the experimental Mo_2AlB_2 XRD pattern, and these impurity peaks around 35° 2θ and 37° 2θ seem to most closely match the peaks of ZnO. Knowing that some oxygen is likely present during the reaction despite attempts to maintain the reaction under nitrogen flow, the oxidation of zinc is not surprising. Furthermore, the presence of ZnO indicates that the zinc is isolated from Mo_2AlB_2, allowing it to oxidize. This result highlights a difference in the reaction mechanisms of MAB phases and MAX phases. While the reaction of Ti_xAlC_{x-1} and $ZnCl_2$ led to Ti_xZnC_{x-1}, the analogous MAB phase reaction between MoAlB and $ZnCl_2$ instead produced Mo_2AlB_2. Furthermore, the metal salt reaction on the MAX phase took 5 hours, while reacting the same metal salt with MoAlB at the same temperature of 550° C took 170 hours. Many reactions between zinc chloride and MoAlB were conducted at shorter time points, but it was consistently observed that the low angle peak was not fully shifted to 15.3° 2θ, which indicated that the reaction had not yet reached Mo_2AlB_2. These differences in reaction and product for the MAB phase MoAlB versus Ti_xAlC_{x-1}, a MAX phase, demonstrate the complex sensitivity of MAB phases compared to MAX phases.

To further investigate the driving forces in the zinc chloride reaction with MoAlB, an experiment was designed to test the impact of melting point of four different metal chloride salts and their redox potential with aluminum. This experiment also provided more insight into the differences between MAX and MAB phases. It has been reported that Lewis acid salt method is generally applicable to MAX phases if the redox potential between the metal salt and the A-element of the MAX phase is positive (i.e. favorable).[27] However, it is unknown whether Lewis acid salt reactions with MAB phases possess the same dependence on redox potential. Powder XRD patterns of the four selected metal chloride salts (Appendix A) along with reference patterns for MoAlB and Mo_2AlB_2 are shown in Figure 5.

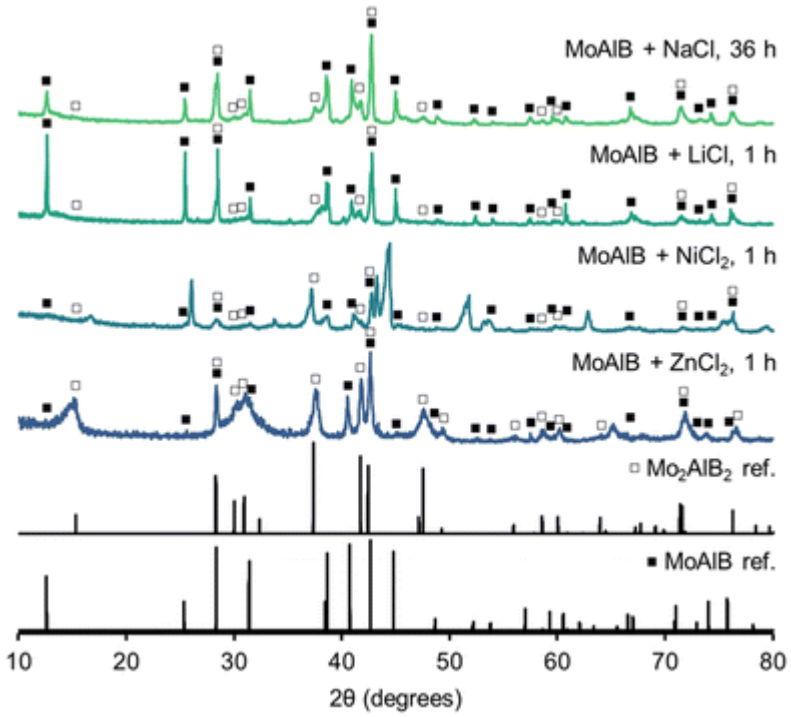

Figure 5. Powder XRD patterns of products of MoAlB and the four selected metal chloride salts. Reference patterns for MoAlB[43] and Mo_2AlB_2[39] are shown and experimental peaks are matched to one of these two patterns. Adapted from Baumler et al.[40]

While the best Mo_2AlB_2 results from the zinc chloride reaction came from a reaction time of 170 hours, in this experiment only short reaction times were necessary to assess whether there

was any indication of Mo_2AlB_2 formation and compare relative reaction speeds. The reaction with $ZnCl_2$, which represents a good redox pair with aluminum and has a low melting point, shows clear signs of Mo_2AlB_2 formation after 1 hour. The shift of the low angle peak toward 15.3° 2θ to match the Mo_2AlB_2 reference pattern is especially indicative that aluminum is being removed and the system is progressing towards Mo_2AlB_2. The reaction with $NiCl_2$ shows lower Mo_2AlB_2 peak intensity compared to $ZnCl_2$, which means that this reaction is likely slower. $NiCl_2$ makes up a favorable redox pair with aluminum and has a high melting point, so this reaction progressing slower than $ZnCl_2$ while still showing signs of aluminum removal aligns with expected results. Interestingly, the two selected metal salts which formed a bad redox pair with aluminum, LiCl and NaCl, also showed preliminary signs of Mo_2AlB_2 formation. Note that in the reaction with NaCl, which has the least favorable reactivity because of Na^+ forming an unfavorable redox pair with aluminum and NaCl's high melting point, there was no sign of Mo_2AlB_2 formation after 1 hour, so the reaction time was increased to 36 hours, at which time early Mo_2AlB_2 formation was visible. Although the low angle peak at 15.3° 2θ which is characteristic of Mo_2AlB_2 does not have notable intensity in either LiCl or NaCl, both reactions display the onset of Mo_2AlB_2 peaks around 30° 2θ and 37° 2θ.

Upon analyzing the XRD patterns of the four metal chloride salts, it does not appear that the redox chemistry between aluminum and the metal salt drives this reaction toward Mo_2AlB_2 as it did for the MAX phase analog. Thus, other potential driving forces should be considered. Chlorine, although present in all the metal chloride salt reactions, does not provide a favorable redox pair with aluminum in this reaction. Chlorine and aluminum don't form a favorable redox pair because, in the general ionic reaction between MCl_x and MoAlB, the MCl_x turns into M^{x+} and Cl^-. Although Cl_2 would be a favorable redox pair, the only known form of chlorine in this

reaction, Cl^-, is not favorable (Table A2). Therefore, it is unlikely that the presence of chlorine is providing the necessary driving force for this reaction. For MAX phases, it has been reported that the aluminum within the MAX phase structure can oxidize to form $AlCl_3$ during etching processes involving HCl[25] and HF[28]. Because $AlCl_3$ is soluble in the solvents used to wash the resulting samples, its presence is rarely observed. Therefore, it is likely that some of the Al in MoAlB oxidizes due to water's presence in the system from the metal salts hydrating. The Al subsequently bonds with the Cl^- of the metal chlorides to form $AlCl_3$ similarly to the MAX phase reactions, and the $AlCl_3$ dissolves in water while the sample is being washed. The observed inhibition of redox chemistry as a driving force for MoAlB with metal chloride salts provides further insight into the intricate differences between MAB and MAX phase synthesis.

3.3 Mo_2AlB_2 from reaction with I_2

After Mo_2AlB_2 was successfully synthesized through a topochemical transformation of MoAlB using $ZnCl_2$, the engineering of alternative synthesis routes was considered. Not only are alternative reaction pathways towards Mo_2AlB_2 valuable from a synthetic perspective, but they also provide the possibility of a slightly altered form of Mo_2AlB_2 which may contain different properties or reactivities. When exploring other possible reactants, one group of chemicals stood out: the halide elements. Fluorine and chlorine have been used effectively as etchants on MAX phases[25,28] and chlorine has also proven effective as a reactant with MoAlB, although to a different level than with MAX phases.[40] Nonetheless, the halide's redox favorability with aluminum makes them a promising option to etch aluminum out of MoAlB and other MAB phases. This understanding warrants the exploration of other halide group elements, namely

bromine and iodine, as reactants. While bromine is of synthetic interest, its high toxicity makes it a non-ideal reactant. As a result, iodine, which has a favorable redox potential when grouped with aluminum, was selected to react with MoAlB in the hopes of forming Mo_2AlB_2 and providing an alternative to the MoAlB and $ZnCl_2$ reaction. A powder XRD pattern of the resulting product is shown in Figure 6, along with the Mo_2AlB_2 via $ZnCl_2$ experimental pattern used in Figure 4 for and reference patterns for MoAlB[43] and Mo_2AlB_2[39] for comparison.

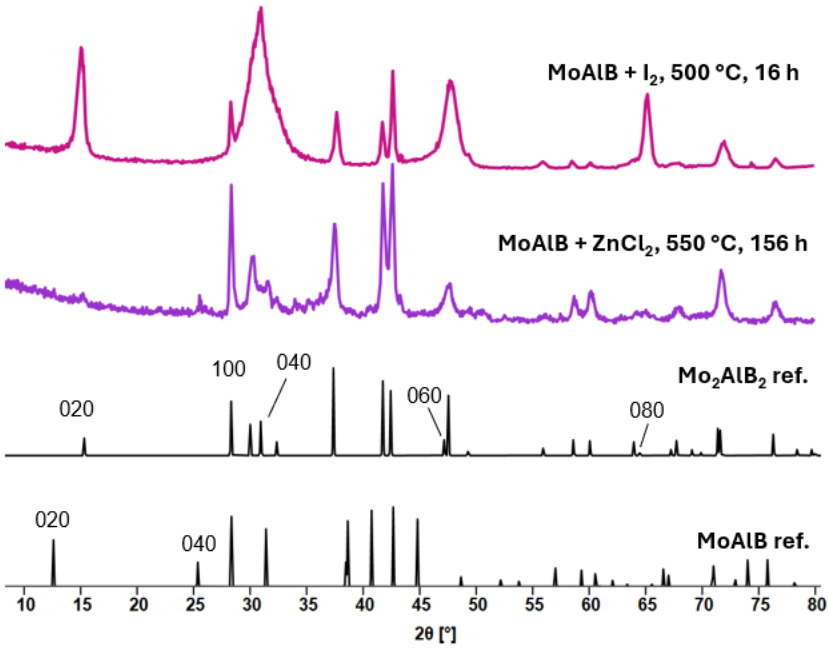

Figure 6. Powder XRD patterns of Mo_2AlB_2 from reaction of MoAlB with $ZnCl_2$ and I_2. Reference patterns for MoAlB[43] and Mo_2AlB_2[39] are shown.

The XRD results for the reaction between MoAlB and iodine in Figure 6 clearly show that Mo_2AlB_2 is being formed. The peaks in the stacking direction (0*k*0, where k is any integer) align very well with the Mo_2AlB_2 reference pattern and the sample also displays the intensity swap of the two peaks around 43° 2θ, which indicates similar stacking faults to those observed in the in the zinc chloride reaction. However, the Mo_2AlB_2 via I_2 displays multiple differences compared to its zinc-chloride-etched counterpart. The most notable difference in the XRD

patterns is the broadness of all peaks in the stacking direction for the iodine reaction pathway, which indicates that there is less order between the layers of Mo_2AlB_2. This disorder could indicate a lower stability Mo_2AlB_2 compared to the Mo_2AlB_2 from $ZnCl_2$, making it more suitable for further aluminum etching. The peaks in the stacking direction for the Mo_2AlB_2 via I_2 also display a considerable increase in peak intensity. Because high peak intensity generally indicates preferred orientation, this result appears contradictory to the broadness of the stacking direction peaks. Alternatively, the simultaneous peak intensity and broadness could signify order within the 2-D layers and disorder between them, meaning that this form of Mo_2AlB_2 is closer to being a 2-D MBene than any previous results. Although further characterization is needed to fully understand the significance of the stacking direction peak intensity and broadness in the iodine version of Mo_2AlB_2, it is currently clear that reacting MoAlB with I_2 results in an altered form of Mo_2AlB_2. The reaction between MoAlB and I_2 is also different from MoAlB and $ZnCl_2$, with the most significant difference being the large reduction in reaction time, which makes Mo_2AlB_2 via I_2 much more time-efficient to synthesize.

To better understand this new form of Mo_2AlB_2 and the forces that drive its synthesis, a temperature series was conducted (Figure 7).

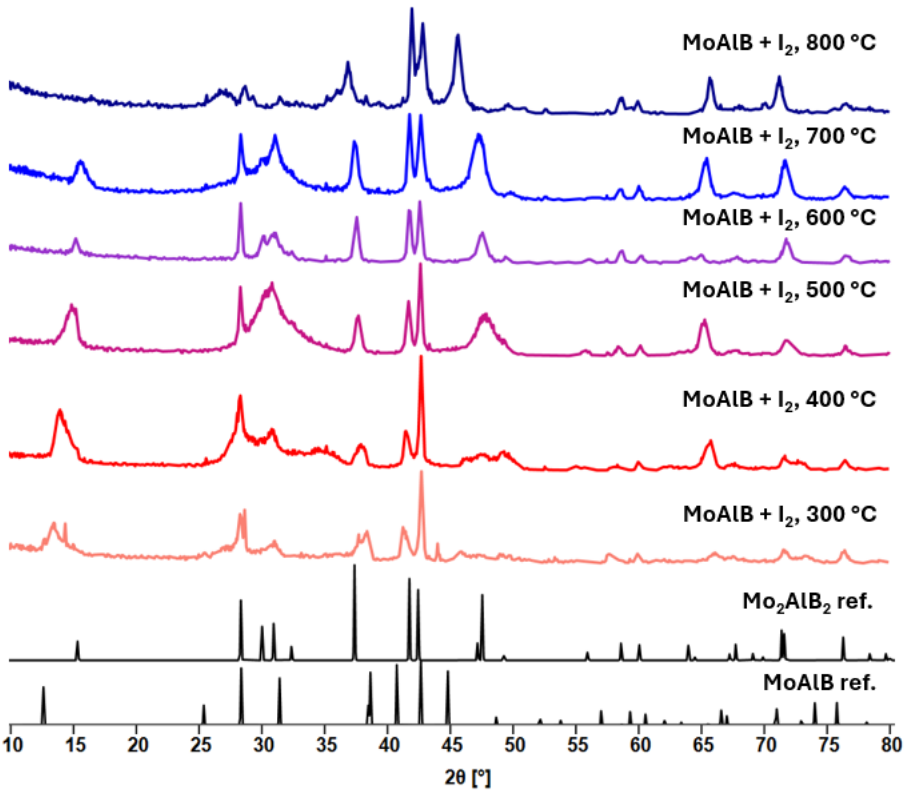

Figure 7. Powder XRD temperature series patterns of the products of I_2 reactions with MoAlB from 300 °C – 800 °C for 16 hours. Reference patterns for MoAlB[43] and Mo_2AlB_2[39] are included.

From Figure 7, it is first observed that within the entire temperature range of 300-800 °C, the reaction between MoAlB and I_2 shows considerable progress towards Mo_2AlB_2. It is also apparent that as the temperature increases from 300-600 °C, a purer form of Mo_2AlB_2 is achieved. This improved structure of Mo_2AlB_2 is indicated by the low angle peak shifting closer and closer to the 15.3° 2θ of the Mo_2AlB_2 reference pattern and improved alignment at most other higher angle peaks. Starting at 700 °C, the two peaks around 43° 2θ revert to the relative peak intensity of the Mo_2AlB_2 reference pattern, thus indicating potential loss of stacking faults. Suppression of the stacking direction likely indicates a loss of order, which could be favorable for aluminum removal or could signify degradation. At 800 °C, degradation of the system is very likely because of the presence of new peaks, namely at 25° 2θ, which indicates new side

products forming. While a certain level of degradation of Mo_2AlB_2 may be necessary to fully remove all aluminum, in this case it appears likely that the degradation is significantly affecting the MoB layers which would result in a damaged and unsignificant product even if the remaining aluminum could be etched. Therefore, the most suitable temperature for the reaction between MoAlB and I_2 is thought to be between 500-600 °C.

3.4 Etching aluminum from Mo_2AlB_2

For MAX phases and MAB phases alike, the selective etching of aluminum is a crucial step to reach 2-D MXenes or MBenes. This step removes the layers of aluminum and weakens the overall crystal structure so that the layers can be exfoliated into 2-D sheets.[26] However, as discussed in Chapter 1.5, MAB phases cannot withstand the harsh etching reactions, typically involving HF, which MAX phases are subjected to.[37] Instead, milder etching reactions, which are still capable of removing aluminum, must be explored. Some such reactions have been used successfully on MAX phases. In Chapter 1.4, a Lewis-acid elemental replacement method[26] and an etching reaction using HCl[25] were reported to successfully remove aluminum in MAX phases. The Lewis-acid approach was shown to behave differently with the MAB phases compared to MAX phases in Chapter 3.2, with zinc chloride removing only half of the aluminum of MoAlB and resulting in Mo_2AlB_2. Although a valuable finding, this means that the Lewis-acid elemental approach is unlikely to fully remove the aluminum from MAB phases. Therefore, HCl was selected as an etching agent on Mo_2AlB_2. For etching reactions, Mo_2AlB_2 is the preferred starting material over MoAlB because half of the aluminum has already been removed and the remaining bonds to aluminum are weaker.[39,40] Aluminum is expected to react with HCl to form

$AlCl_3$, the same side product formed in the zinc chloride reactions. Recognizing aluminum's amphoteric nature, meaning that it can act as an acid or a base, NaOH, a strong base, was selected as a potential etchant in addition to HCl.

Figure 8 shows the products formed from stirring Mo_2AlB_2 in HCl and NaOH, respectively, at room temperature. Although there are not major changes in the two patterns where etching is anticipated compared to the starting Mo_2AlB_2 sample, there are subtle differences which could indicate some degree of etching.

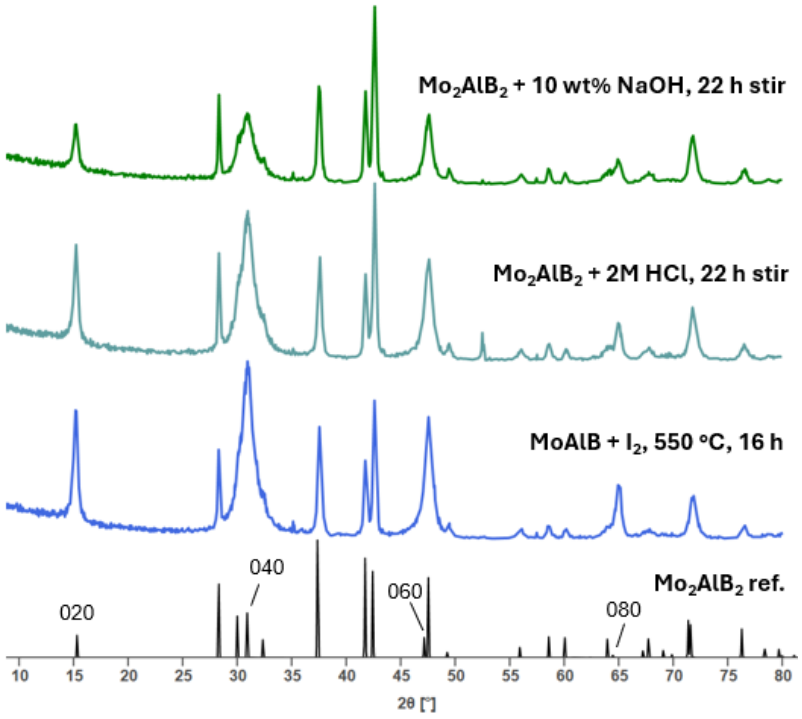

Figure 8. Powder XRD patterns of the products of Mo_2AlB_2 stirring in HCl and NaOH. The pattern of the starting Mo_2AlB_2 sample and the reference pattern for Mo_2AlB_2[39] are included.

There is little to no peak shifting among the acid and base stirred patterns, but there is noticeable suppression of the peaks in the stacking direction, which are labeled on the Mo_2AlB_2 reference pattern. These peaks are more suppressed in the NaOH-etched pattern than the HCl-etched pattern. Although it is hard to know what this peak suppression means, peak intensity is often

associated with order in a crystalline structure, so the lack thereof could indicate a loss of order because of aluminum removal. Previous reactions with MoAlB have never been pushed beyond the metastable well that Mo_2AlB_2 lies in, meaning that even a small amount of additional aluminum removal from an Mo_2AlB_2 starting material is a new and exciting discovery. It is also noteworthy that both etching reactions proceeded at room temperature. While the previously reported reactions with MoAlB using zinc chloride and iodine only reacted with the aluminum at high temperatures, here we observe reactions that can occur at room temperature. One possible reason for this difference is that both HCl and NaOH dissociate in water, which means that the free ions are readily available to react with aluminum instead of needing a redox reaction to free them.

To assess the quality of the samples and analyze differences between the two etchants, further characterization was done on the etched Mo_2AlB_2 samples using SEM (Figure 9).

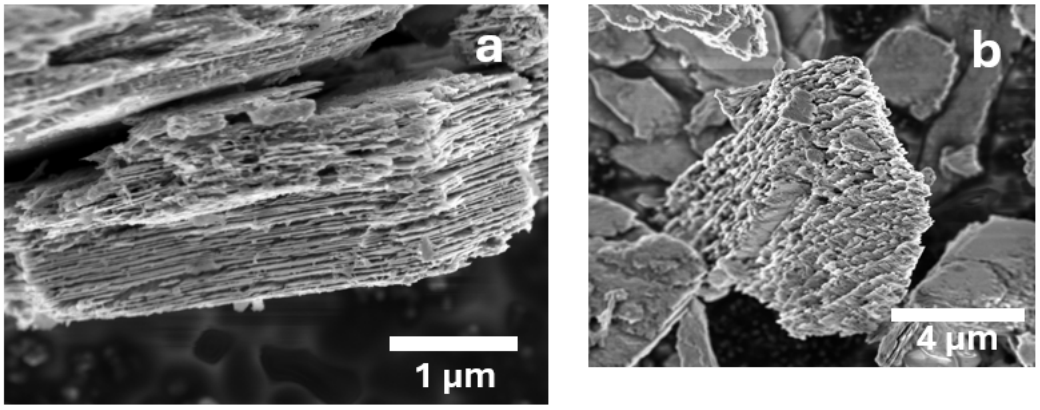

Figure 9. (a) SEM image of etched Mo_2AlB_2 from stirring Mo_2AlB_2 in 2M HCl. (b) SEM image of etched Mo_2AlB_2 from stirring Mo_2AlB_2 in 10 weight-percent NaOH.

From Figure 9b, it is apparent that the NaOH-etched sample shows signs of surface degradation. This can be seen by the wavy patterns forming on the top and sides of the crystal. Gaps between MoB layers are still visible, but the high degree of surface degradation indicates that NaOH is

reacting with more than just aluminum and lowering the quality of the remaining molybdenum boride sheets. Because some aluminum is still expected to be in the sample based on XRD, trying to remove further aluminum using NaOH is likely to further destroy the sample. Alternatively, the sample that was stirred in HCl appears relatively pristine. There still appears to be some degradation on the edges of the molybdenum boride layers, but the gaps between these layers are much more pronounced and consistent. Therefore, it appears that while both NaOH and HCl effectively remove aluminum from Mo_2AlB_2, HCl does so in a less destructive manner.

Chapter 4:

Conclusion

Batteries, and specifically LIBs, are used in almost every aspect of day-to-day life.[2] The need for more renewable energy, such as solar and wind power, makes batteries even more important, as batteries are seen as a viable option for grid-scale energy storage.[1] However, current LIBs and other batteries come with many shortcomings such as combustibility and dependence on a finite supply of natural materials.[2] Batteries may be the future, but there is a need to improve batteries to ensure that future is a bright one. Most LIBs currently use graphene as an electrode material.[8] Graphene is part of a family of materials that are called 2-D, meaning that they have been reduced to single layers from their 3-D structured precursors.[5] However, graphene is not the only 2-D material that could be employed in LIBs, and it may not even be the best. Enter MAX phases and MAB phases, two closely related families of 3-D materials that have gained significant attention because of their 2-D counterparts, MXenes and MBenes. Many different MXenes have already been synthesized, and their electric properties are exceptional. MBenes, however, have only come into the light because of MAX phase and MXene synthetic success, and much less success has been achieved on this family of 2-D materials. However, their theoretically predicted properties are just as promising as MXenes, if not more.

This thesis focuses on engineering different reaction pathways on the MAB phase MoAlB toward the 2-D MoB MBene. While most attempted pathways resulted in the metastable phase, Mo_2AlB_2, instead of a 2-D MBene, etching reactions on Mo_2AlB_2 using HCl showed signs of further aluminum removal by XRD analysis. This additional aluminum etching past Mo_2AlB_2 indicates that a multi-step topochemical reaction, wherein high-quality Mo_2AlB_2 is first

synthesized and then further etched, could be a promising pathway towards the MoB MBene. In addition, the two topochemical reactions using $ZnCl_2$ and I_2 to form Mo_2AlB_2 provide insight into a relatively new field of materials and illuminate the differences between MAX phases and MAB phases. Understanding these differences will be crucial for the synthesis of other MAB phases as well as successful engineering of pathways toward 2-D MBenes. To further understand the unique synthetic properties of MoAlB and other MAB phases, future work will likely involve experimenting with different synthetic approaches to reach Mo_2AlB_2 and different etching methods. Although the next steps focus on the synthetic side of the MoB MBene, if this 2-D material can be synthesized, there will be much research applied toward examining its mechanical and electrical properties and analyzing its use as an electrode material for the batteries of the future.

Appendix A:

Justification for Metal Chloride Salt Selection

To study the impact of melting point and electrochemical potential (i.e. favorability) on the zinc chloride reaction toward Mo_2AlB_2, three metal chloride salts were selected. First, using a standard redox potential table, metal chloride salts which had a negative potential when reacted with aluminum (unfavorable) and which had a positive potential (favorable) were identified and grouped. Next, with a reaction temperature defined at 650 °C, a metal chloride salt with a melting point greater than the reaction temperature and another metal chloride salt with a melting point below the reaction temperature was selected from both the favorable and unfavorable groups of reactants.

Table A1. Summary of selected metal chloride salts based on melting point[45] and reactivity, which is determined by redox potential, E(V).

Melting Point (MP)	Reactivity with aluminum	
	Favorable (E(V) > 0)	Unfavorable (E(V) < 0)
MP > 650 °C	$NiCl_2$ (MP: 1000 °C, E: 2.48 V)	NaCl (MP: 800 °C, E: -6.47 V)
MP < 650 °C	$ZnCl_2$ (MP: 290 °C, E: 1.04 V)	LiCl (MP: 605 °C, E: -7.49 V)

$ZnCl_2$ was used as the favorable metal chloride salt with a melting point below the reaction temperature. The other three selected metal chloride salts were $NiCl_2$, LiCl, and NaCl. Table 1

provides a summary of the four selected metal chloride salts with respect to melting point and reactivity.

Table A2. Calculations for Redox Potentials of Selected Metals and Chlorine with Aluminum.

Redox Couple with Aluminum	Redox Reaction and Potentials (V)		Overall Redox Potential (V)
Lithium (Li)	$(Li^+(aq) + e^- \rightarrow Li(s))3$ $Al(s) \rightarrow Al^{3+}(aq) + 3e^-$	3(-3.05) 1.66	-7.49
Sodium (Na)	$(Na^+(aq) + e^- \rightarrow Na(s))3$ $Al(s) \rightarrow Al^{3+}(aq) + 3e^-$	3(-2.71) 1.66	-6.47
Zinc (Zn)	$(Zn^{2+}(aq) + 2e^- \rightarrow Zn(s))3$ $(Al(s) \rightarrow Al^{3+}(aq) + 3e^-)2$	3(-0.76) 2(1.66)	1.04
Nickel (Ni)	$(Ni^{2+}(aq) + 2e^- \rightarrow Ni(s))3$ $(Al(s) \rightarrow Al^{3+}(aq) + 3e^-)2$	3(-0.28) 2(1.66)	2.48
Chlorine (Cl)	$(2Cl^-(g) \rightarrow Cl_2(aq) + 2e^-)3$ $(Al(s) \rightarrow Al^{3+}(aq) + 3e^-)2$	3(-1.36) 2(1.66)	-0.76

Appendix B:

Simulating Preferred Orientation on Reference Patterns for MoAlB and Mo_2AlB_2

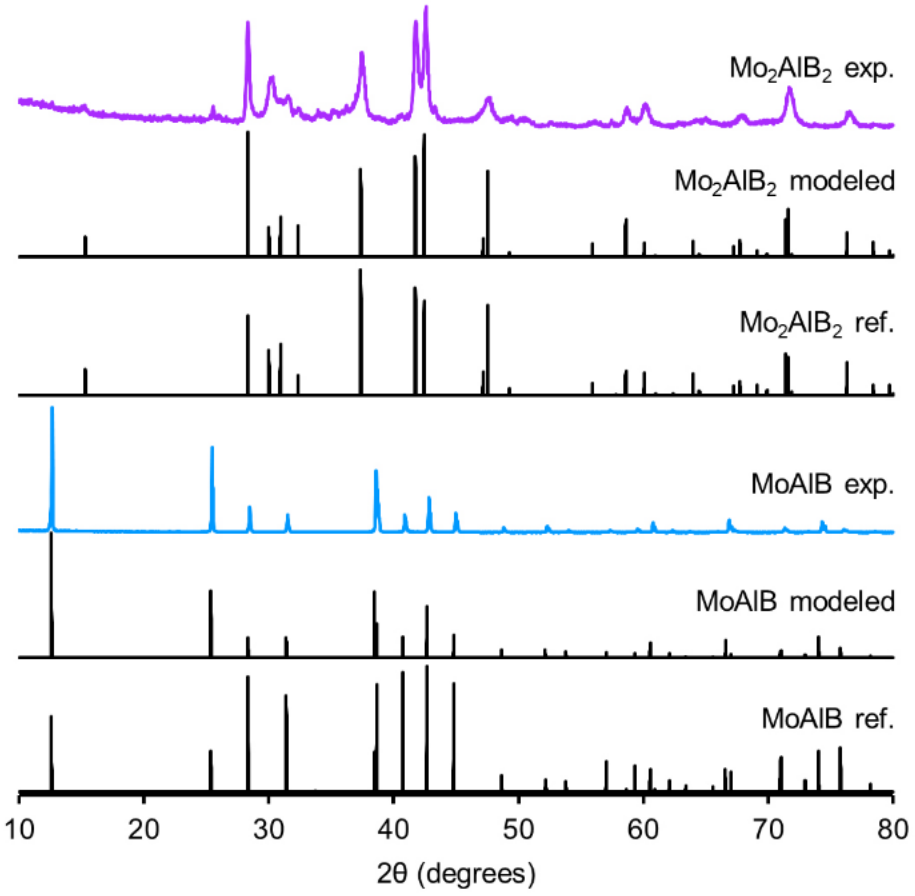

Figure B1. Powder XRD patterns of Mo_2AlB_2 (purple) synthesized by reacting MoAlB (blue) with $ZnCl_2$ at 550°C for 170 hours. Reference patterns based on published crystallographic data for MoAlB[43] and Mo_2AlB_2[39]. Modeled patterns display preferred orientation in 0k0 for MoAlB and 021 for Mo_2AlB_2. Adapted from Baumler et al.[40]

Figure B1 highlights the adjustments to the original reference patterns for MoAlB[43] and Mo_2AlB_2[39] to account for preferred orientation. The resulting simulated patterns appear in Figure 4. Modeling the MoAlB reference pattern with preferred orientation in the 0*k*0 direction was a clear choice due to the high peak intensity of the 020 and 040 peaks in the experimental MoAlB.

Modeling preferred orientation in the 021 direction for Mo_2AlB_2, although a less clear choice, was effective in displaying suppression in the *h*00 direction without affecting the 00*l* direction. This adjustment provides a simulated pattern with swapped peak intensity for the two peaks around 43° 2θ, which matches the stacking faults in the observed experimental pattern.

BIBLIOGRAPHY

(1) Dunn, B.; Kamath, H.; Tarascon, J.-M. Electrical Energy Storage for the Grid: A Battery of Choices. *Science* **2011**, *334* (6058), 928–935. https://doi.org/10.1126/science.1212741.

(2) Armand, M.; Tarascon, J.-M. Building Better Batteries. *Nature* **2008**, *451* (7179), 652–657. https://doi.org/10.1038/451652a.

(3) Flowers, P.; Theopold, K.; Langley, R.; Robinson, W. R. *Chemistry 2e*. https://openstax.org/ (accessed 2024-10-03).

(4) Kirchev, A. Chapter 20 - Battery Management and Battery Diagnostics. In *Electrochemical Energy Storage for Renewable Sources and Grid Balancing*; Moseley, P. T., Garche, J., Eds.; Elsevier: Amsterdam, 2015; pp 411–435. https://doi.org/10.1016/B978-0-444-62616-5.00020-6.

(5) Choi, W.; Lahiri, I.; Seelaboyina, R.; Kang, Y. S. Synthesis of Graphene and Its Applications: A Review. **2010**.

(6) Bonaccorso, F.; Colombo, L.; Yu, G.; Stoller, M.; Tozzini, V.; Ferrari, A. C.; Ruoff, R. S.; Pellegrini, V. Graphene, Related Two-Dimensional Crystals, and Hybrid Systems for Energy Conversion and Storage. *Science* **2015**, *347* (6217), 1246501. https://doi.org/10.1126/science.1246501.

(7) Chen, K.-S.; Balla, I.; Luu, N. S.; Hersam, M. C. Emerging Opportunities for Two-Dimensional Materials in Lithium-Ion Batteries. *ACS Energy Lett.* **2017**, *2* (9), 2026–2034. https://doi.org/10.1021/acsenergylett.7b00476.

(8) Bonaccorso, F.; Lombardo, A.; Hasan, T.; Sun, Z.; Colombo, L.; Ferrari, A. C. Production and Processing of Graphene and 2d Crystals. *Materials Today* **2012**, *15* (12), 564–589. https://doi.org/10.1016/S1369-7021(13)70014-2.

(9) Stankovich, S.; Dikin, D. A.; Dommett, G. H. B.; Kohlhaas, K. M.; Zimney, E. J.; Stach, E. A.; Piner, R. D.; Nguyen, S. T.; Ruoff, R. S. Graphene-Based Composite Materials. *Nature* **2006**, *442* (7100), 282–286. https://doi.org/10.1038/nature04969.

(10) Anasori, B.; Lukatskaya, M. R.; Gogotsi, Y. 2D Metal Carbides and Nitrides (MXenes) for Energy Storage. *Nat Rev Mater* **2017**, *2* (2), 1–17. https://doi.org/10.1038/natrevmats.2016.98.

(11) Gogotsi, Y.; Anasori, B. The Rise of MXenes. *ACS Nano* **2019**, *13* (8), 8491–8494. https://doi.org/10.1021/acsnano.9b06394.

(12) Shah, S. A.; Habib, T.; Gao, H.; Gao, P.; Sun, W.; Green, M. J.; Radovic, M. Template-Free 3D Titanium Carbide (Ti3C2Tx) MXene Particles Crumpled by Capillary Forces. *Chem. Commun.* **2016**, *53* (2), 400–403. https://doi.org/10.1039/C6CC07733A.

(13) Chaudhari, N. K.; Jin, H.; Kim, B.; Baek, D. S.; Joo, S. H.; Lee, K. MXene: An Emerging Two-Dimensional Material for Future Energy Conversion and Storage Applications. *J. Mater. Chem. A* **2017**, *5* (47), 24564–24579. https://doi.org/10.1039/C7TA09094C.

(14) Zhao, X.; Liu, M.; Chen, Y.; Hou, B.; Zhang, N.; Chen, B.; Yang, N.; Chen, K.; Li, J.; An, L. Fabrication of Layered Ti3C2 with an Accordion-like Structure as a Potential Cathode Material for High Performance Lithium–Sulfur Batteries. *J. Mater. Chem. A* **2015**, *3* (15), 7870–7876. https://doi.org/10.1039/C4TA07101H.

(15) Liang, X.; Garsuch, A.; Nazar, L. F. Sulfur Cathodes Based on Conductive MXene Nanosheets for High-Performance Lithium–Sulfur Batteries. *Angewandte Chemie International Edition* **2015**, *54* (13), 3907–3911. https://doi.org/10.1002/anie.201410174.
(16) Naguib, M.; Come, J.; Dyatkin, B.; Presser, V.; Taberna, P.-L.; Simon, P.; Barsoum, M. W.; Gogotsi, Y. MXene: A Promising Transition Metal Carbide Anode for Lithium-Ion Batteries. *Electrochemistry Communications* **2012**, *16* (1), 61–64. https://doi.org/10.1016/j.elecom.2012.01.002.
(17) Dall'Agnese, Y.; Taberna, P.-L.; Gogotsi, Y.; Simon, P. Two-Dimensional Vanadium Carbide (MXene) as Positive Electrode for Sodium-Ion Capacitors. *J. Phys. Chem. Lett.* **2015**, *6* (12), 2305–2309. https://doi.org/10.1021/acs.jpclett.5b00868.
(18) Xie, Y.; Dall'Agnese, Y.; Naguib, M.; Gogotsi, Y.; Barsoum, M. W.; Zhuang, H. L.; Kent, P. R. C. Prediction and Characterization of MXene Nanosheet Anodes for Non-Lithium-Ion Batteries. *ACS Nano* **2014**, *8* (9), 9606–9615. https://doi.org/10.1021/nn503921j.
(19) Wyatt, B. C.; Rosenkranz, A.; Anasori, B. 2D MXenes: Tunable Mechanical and Tribological Properties. *Advanced Materials* **2021**, *33* (17), 2007973. https://doi.org/10.1002/adma.202007973.
(20) Zhou, A.; Wang, C.-A.; Hunag, Y. Synthesis and Mechanical Properties of Ti3AlC2 by Spark Plasma Sintering. *Journal of Materials Science* **2003**, *38* (14), 3111–3115. https://doi.org/10.1023/A:1024777213910.
(21) Tzenov, N. V.; Barsoum, M. W. Synthesis and Characterization of Ti3AlC2. *Journal of the American Ceramic Society* **2000**, *83* (4), 825–832. https://doi.org/10.1111/j.1151-2916.2000.tb01281.x.
(22) Haemers, J.; Gusmão, R.; Sofer, Z. Synthesis Protocols of the Most Common Layered Carbide and Nitride MAX Phases. *Small Methods* **2020**, *4* (3), 1900780. https://doi.org/10.1002/smtd.201900780.
(23) Gauthier, V.; Cochepin, B.; Dubois, S.; Vrel, D. Self-Propagating High-Temperature Synthesis of Ti3SiC2: Study of the Reaction Mechanisms by Time-Resolved X-Ray Diffraction and Infrared Thermography. *Journal of the American Ceramic Society* **2006**, *89* (9), 2899–2907. https://doi.org/10.1111/j.1551-2916.2006.01120.x.
(24) Etzkorn, J.; Ade, M.; Hillebrecht, H. V2AlC, V4AlC3-x (x ≈ 0.31), and V12Al3C8: Synthesis, Crystal Growth, Structure, and Superstructure. *Inorg. Chem.* **2007**, *46* (18), 7646–7653. https://doi.org/10.1021/ic700382y.
(25) Wang, C.; Shou, H.; Chen, S.; Wei, S.; Lin, Y.; Zhang, P.; Liu, Z.; Zhu, K.; Guo, X.; Wu, X.; Ajayan, P. M.; Song, L. HCl-Based Hydrothermal Etching Strategy toward Fluoride-Free MXenes. *Advanced Materials* **2021**, *33* (27), 2101015. https://doi.org/10.1002/adma.202101015.
(26) Li, M.; Lu, J.; Luo, K.; Li, Y.; Chang, K.; Chen, K.; Zhou, J.; Rosen, J.; Hultman, L.; Eklund, P.; Persson, P. O. Å.; Du, S.; Chai, Z.; Huang, Z.; Huang, Q. Element Replacement Approach by Reaction with Lewis Acidic Molten Salts to Synthesize Nanolaminated MAX Phases and MXenes. *J. Am. Chem. Soc.* **2019**, *141* (11), 4730–4737. https://doi.org/10.1021/jacs.9b00574.
(27) Li, Y.; Shao, H.; Lin, Z.; Lu, J.; Liu, L.; Duployer, B.; Persson, P. O. Å.; Eklund, P.; Hultman, L.; Li, M.; Chen, K.; Zha, X.-H.; Du, S.; Rozier, P.; Chai, Z.; Raymundo-Piñero, E.; Taberna, P.-L.; Simon, P.; Huang, Q. A General Lewis Acidic Etching Route for

Preparing MXenes with Enhanced Electrochemical Performance in Non-Aqueous Electrolyte. *Nat. Mater.* **2020**, *19* (8), 894–899. https://doi.org/10.1038/s41563-020-0657-0.
(28) Srivastava, P.; Mishra, A.; Mizuseki, H.; Lee, K.-R.; Singh, A. K. Mechanistic Insight into the Chemical Exfoliation and Functionalization of Ti3C2 MXene. *ACS Appl. Mater. Interfaces* **2016**, *8* (36), 24256–24264. https://doi.org/10.1021/acsami.6b08413.
(29) Mashtalir, O.; Naguib, M.; Mochalin, V. N.; Dall'Agnese, Y.; Heon, M.; Barsoum, M. W.; Gogotsi, Y. Intercalation and Delamination of Layered Carbides and Carbonitrides. *Nat Commun* **2013**, *4* (1), 1716. https://doi.org/10.1038/ncomms2664.
(30) Naguib, M.; R. Unocic, R.; L. Armstrong, B.; Nanda, J. Large-Scale Delamination of Multi-Layers Transition Metal Carbides and Carbonitrides "MXenes." *Dalton Transactions* **2015**, *44* (20), 9353–9358. https://doi.org/10.1039/C5DT01247C.
(31) Wang, J.; Ye, T.-N.; Gong, Y.; Wu, J.; Miao, N.; Tada, T.; Hosono, H. Discovery of Hexagonal Ternary Phase Ti2InB2 and Its Evolution to Layered Boride TiB. *Nat Commun* **2019**, *10* (1), 2284. https://doi.org/10.1038/s41467-019-10297-8.
(32) Zhou, J.; Palisaitis, J.; Halim, J.; Dahlqvist, M.; Tao, Q.; Persson, I.; Hultman, L.; Persson, P. O. Å.; Rosen, J. Boridene: Two-Dimensional Mo4/3B2-x with Ordered Metal Vacancies Obtained by Chemical Exfoliation. *Science* **2021**, *373* (6556), 801–805. https://doi.org/10.1126/science.abf6239.
(33) Guo, Z.; Zhou, J.; Sun, Z. New Two-Dimensional Transition Metal Borides for Li Ion Batteries and Electrocatalysis. *J. Mater. Chem. A* **2017**, *5* (45), 23530–23535. https://doi.org/10.1039/C7TA08665B.
(34) Jia, J.; Li, B.; Duan, S.; Cui, Z.; Gao, H. Monolayer MBenes: Prediction of Anode Materials for High-Performance Lithium/Sodium Ion Batteries. *Nanoscale* **2019**, *11* (42), 20307–20314. https://doi.org/10.1039/C9NR05708K.
(35) Sharma, A.; Rangra, V. S.; Thakur, A. Synthesis, Properties, and Applications of MBenes (Two-Dimensional Metal Borides) as Emerging 2D Materials: A Review. *J Mater Sci* **2022**, *57* (27), 12738–12751. https://doi.org/10.1007/s10853-022-07378-3.
(36) Guo, Z.; Zhang, L.; Azam, T.; Wu, Z.-S. Recent Advances and Key Challenges of the Emerging MBenes from Synthesis to Applications. *MetalMat* **2024**, *1* (1), e12. https://doi.org/10.1002/metm.12.
(37) Alameda, L. T.; Holder, C. F.; Fenton, J. L.; Schaak, R. E. Partial Etching of Al from MoAlB Single Crystals To Expose Catalytically Active Basal Planes for the Hydrogen Evolution Reaction. *Chem. Mater.* **2017**, *29* (21), 8953–8957. https://doi.org/10.1021/acs.chemmater.7b02511.
(38) Alameda, L. T.; Moradifar, P.; Metzger, Z. P.; Alem, N.; Schaak, R. E. Topochemical Deintercalation of Al from MoAlB: Stepwise Etching Pathway, Layered Intergrowth Structures, and Two-Dimensional MBene. *J. Am. Chem. Soc.* **2018**, *140* (28), 8833–8840. https://doi.org/10.1021/jacs.8b04705.
(39) Alameda, L. T.; Lord, R. W.; Barr, J. A.; Moradifar, P.; Metzger, Z. P.; Steimle, B. C.; Holder, C. F.; Alem, N.; Sinnott, S. B.; Schaak, R. E. Multi-Step Topochemical Pathway to Metastable Mo2AlB2 and Related Two-Dimensional Nanosheet Heterostructures. *J. Am. Chem. Soc.* **2019**, *141* (27), 10852–10861. https://doi.org/10.1021/jacs.9b04726.
(40) J. Baumler, K.; S. Adams, O.; E. Schaak, R. One-Step Topochemical Transformation of MoAlB into Metastable Mo 2 AlB 2 Using a Metal Chloride Salt Reaction. *Chemical Communications* **2023**, *59* (32), 4814–4817. https://doi.org/10.1039/D3CC00138E.

(41) PubChem. *Zinc Chloride*. https://pubchem.ncbi.nlm.nih.gov/compound/5727 (accessed 2024-10-23).
(42) CrystalDiffract Software Ltd.
(43) Jeitschko, W. Die Kristallstruktur von MoAlB. *Monatshefte für Chemie* **1966**, *97* (5), 1472–1476. https://doi.org/10.1007/BF00902599.
(44) CrystalMaker Software Ltd.
(45) Informatics, N. O. of D. and. *NIST Chemistry WebBook*. https://webbook.nist.gov/chemistry/ (accessed 2024-11-04).

Academic Vita
Owen Adams

EDUCATION

Bachelor of Science with Honors in Mechanical Engineering — Aug 2021 – May 2025
The Pennsylvania State University, Schreyer Honors College — University Park, PA
- Evan Pugh Award Recipient Spring 2024

Jönköping University – Penn State Education Abroad — Jan 2024 – June 2024, Jönköping, Sweden

WORK EXPERIENCE

Ski Instructor, Tussey Mountain — Dec 2024 – Mar 2025, State College, PA
- Using interpersonal skills to communicate complex ideas to students and collaborate with other instructors effectively

Energy Engineering Assistant, Envinity Building Energy Solutions — May 2023 – Aug 2023, State College, PA
- Led independent research and development project to effectively cross-reference data between clients
- Performed data analytics on energy consumption for major healthcare facilities such as Cleveland Clinic and Baptist Health

RESEARCH EXPERIENCE

Undergraduate Researcher, Penn State Chemistry Department — Jul 2022 – May 2025, University Park, PA
- Working to synthesize new 2-D materials with promising characteristics in energy storage
- Responsible for conducting experimental reactions and analyzing resulting samples

Publications

Baumler, Kate; **Adams, Owen**; Schaak, Raymond E. 'One-step topochemical transformation of MoAlB into metastable Mo_2AlB_2 using a metal chloride salt reaction'. *Chem. Commun.* 2023, 59, 4814-4817.

SCHOLARSHIPS

Schreyer Honors College Gatehouse Scholarship — Fall 2022, Spring 2023
Hogan and Grace Markle Scholarship — Spring 2021

SKILLS

MS Office, AutoCAD, SolidWorks, MATLAB

INTERESTS

Sustainable Design, Innovative Materials, Renewable Energy, Global Experiences